Self-generated magnetic dipoles in weakly magnetized beam-plasma system

Qing Jia,[1,2] Kunioki Mima,[2,3,*] Hong-bo Cai,[1,4,†] Toshihiro Taguchi,[5] Hideo Nagatomo,[2] and X. T. He[1,4]

[1]*HEDPS, Center for Applied Physics and Technology, Peking University, Beijing 100871, China*

[2]*Institute of Laser Engineering, Osaka University, Osaka 565-0871, Japan*

[3]*Graduate School for the Creation of New Photonics Industries, Hamamatsu 431-1202, Japan*

[4]*Institute of Applied Physics and Computational Mathematics, Beijing 100094, China*

[5]*Department of Electric and Electronic Engineering, Setsunan University, Osaka 572-8508, Japan*

(Received 10 July 2014; published 24 February 2015)

A self-generation mechanism of magnetic dipoles and the anomalous energy dissipation of fast electrons in a magnetized beam-plasma system are presented. Based on two-dimensional particle-in-cell simulations, it is found that the magnetic dipoles are self-organized and play important roles in the beam electron energy dissipation. These dipoles drift slowly in the direction of the return flow with a quasisteady velocity, which depends upon the magnetic amplitude of the dipole and the imposed external magnetic field. This dipole formation provides a mechanism for the anomalous energy dissipation of a relativistic electron beam, which would play an important role in collisionless shock and ion shock acceleration.

DOI: 10.1103/PhysRevE.91.023107 PACS number(s): 52.57.Kk, 52.35.Qz, 52.65.Rr

I. INTRODUCTION

The relativistic counterstreaming beam-plasma system is a fundamental issue in plasma physics. It is unstable to the well-known two-stream instability (TSI) [1] and Weibel instability (WI) [2], which are of wide relevance to many fields like fusion physics and astrophysics. In the fast ignition scenario (FIS) of laser inertial confinement fusion, the flow of hot electrons penetrates into the cold background plasma and generates neutralizing return currents. The resultant unstable electromagnetic Weibel instability in this counterstreaming system contributes to the anomalous stopping of fast electrons [3]. Namely, both the beam and background electrons are statistically scattered by the magnetic fluctuations, which increases the beam electron divergence [4]. In addition, the Weibel instability is also believed to be the mechanism for the formation of collisionless shocks in astrophysics [5] and the shock structure is sensitive to the ambient magnetic fields of the plasma [6]. Recently, a strong external magnetic field of the order of kiloteslas has already been produced in experiments [7], which could be applied to guide the fast electrons [8] in the magnetized FIS [9], and also to facilitate the study of astrophysical shocks in the laboratory [10].

Previously, a variety of theoretical studies [11–14] has demonstrated abundant interesting nonlinear phenomena such as the generation of magnetic dipoles (MDs) in an unstable beam-plasma system. For example, two-dimensional (2D) particle-in-cell (PIC) simulations of ultraintense laser-plasma interaction show a row of MDs trailing the laser pulse in an underdense plasma [11], as well as one solitary magnetic dipole accelerating ions in a moderate-density plasma [12]. A kinetic 2D Vlasov simulation was also employed to investigate the dynamics of a nonrelativistic localized electron beam in plasma, and a chain of MDs were found to form based on resonant wave-particle interactions [13]. Despite all these pioneering works, which were mainly focused on the electromagnetic evolutions of a single electron beam that is initially localized in unmagnetized plasmas, further investigations of the nonlinear interaction of a relativistic electron beam with magnetized dense plasma are needed.

In this paper, we investigate the evolution of a homogeneously distributed beam-plasma system to observe the self-generation of MDs in a weakly magnetized plasma at the nonlinear stage of the Weibel instability. The propagation and amplification of these MDs contribute to the enhanced energy dissipation of the beam electrons, which may provide the explanation for the anomalous stopping of fast electron beams in a weakly magnetized plasma, as indicated by the results of the hybrid simulation performed by Taguchi [15], and also provide further insights in the study of the formation of collisionless shocks and relevant shock acceleration [16]. In addition, to study the transport process under more realistic conditions, we also simulate the interaction of an ultraintense laser pulse with a preionized weakly magnetized plasma to examine the generation of MDs and their effects on fast electron generation and transport.

II. PARTICLE-IN-CELL SIMULATIONS FOR A COUNTERSTREAMING SYSTEM

We use the 2D PIC simulation code ASCENT [17] to study the transport of relativistic electron beams in magnetized dense plasmas. The simulation plane is parallel to the beam propagation direction as well as to the direction of the external magnetic field $B_0\hat{x}$. All quantities in the simulations are normalized to the plasma frequency $\omega_{pe} = (4\pi n_e e^2/m_e)^{1/2}$ and the collisionless skin depth c/ω_{pe}, and, consequently, fields are normalized to the characteristic field $m_e c\omega_{pe}/e$. Here e and m_e denote the charge and mass of the electron, c the light velocity, and n_e the total density of the electrons. The simulation region is $25.6\lambda_0$ ($\lambda_0 = 2\pi c/\omega_{pe}$) in the x direction and $12.8\lambda_0$ in the y direction with 1024×512 cells. Periodic boundary conditions are applied for particles and fields in both directions. 100 particles per cell are used for both the beam and

*mima@ile.osaka-u.ac.jp

†cai_hongbo@iapcm.ac.cn

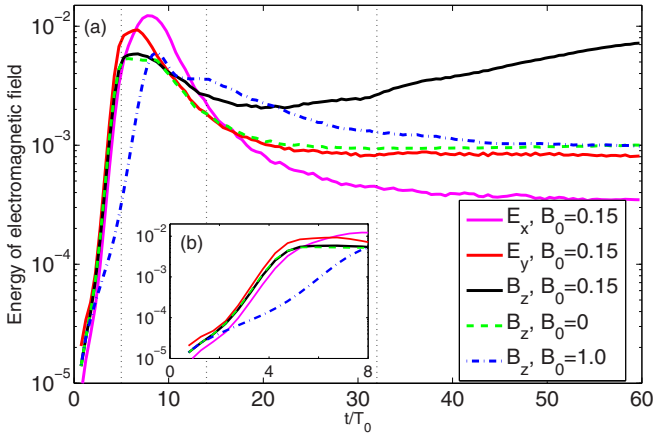

FIG. 1. (Color online) (a) The temporal evolution of the energy of B_z for cases with external magnetic fields of $\mathbf{B}_0 = 0$ (green dashed line), $\mathbf{B}_0 = 0.15$ (black solid line), and $\mathbf{B}_0 = 1.0$ (blue dash-dotted line), and the energy of E_x (magenta solid line) and E_y (red solid line) for the $\mathbf{B}_0 = 0.15$ case. The inserted figure (b) shows the temporal evolutions in the linear stage.

the background electrons with immobile ions. The density ratio of the beam and background electrons is $n_b/n_p = 1/6$ with the drift velocities of $\mathbf{v}_b = 0.978c$ for the beam and $\mathbf{v}_p = -0.163c$ for the background electrons; thus $n_b\mathbf{v}_b + n_p\mathbf{v}_p = 0$. The total simulation time is $60T_0$ ($T_0 = 2\pi/\omega_{pe}$). In order to reduce the restrictions on the grid size compared with the Debye length, the fields and currents in the simulations are evaluated by a fourth-order interpolation scheme [18]. We have performed a number of simulations without and with external magnetic fields of different amplitudes.

Figure 1(a) shows the temporal evolutions of the total energy of the out-of-plane magnetic field B_z ($\int B_z^2/8\pi dV = \langle B_z^2\rangle$) and the electric field E_y ($\int E_y^2/8\pi dV$) and E_x ($\int E_x^2/8\pi dV$), which are normalized to the initial total kinetic energy in the system for simulations with different amplitudes of external magnetic field. In the linear stage of the instabilities, the field energies grow exponentially at almost the same growth rate for $\mathbf{B}_0 = 0.15$ and $\mathbf{B}_0 = 0$, as shown in Fig. 1(b). In the case with strong external magnetic field ($\mathbf{B}_0 = 1.0$), the growth rate is smaller than in the weakly magnetized cases [19]. The growth rates calculated from the energy buildup rates in simulations approximately agree with the maximum growth rates [$0.3\omega_{pe}$ (oblique TSI) for $\mathbf{B}_0 = 0$ and $0.2\omega_{pe}$ (oblique TSI) for $\mathbf{B}_0 = 1.0$] calculated by using the dispersion relation of Ref. [20]. After $t = 5T_0$, the instabilities are saturated by the momentum spread of both the beam and background electrons. In particular, the growth of the short-wavelength modes is significantly suppressed by this thermalization. After saturation, the electric current and B_z field fluctuations are damped by the anomalous viscosity $\mu = \langle v_f^2\rangle\tau$, and the magnetic energy decays rapidly as shown in Fig. 1(a). Here, $\langle v_f^2\rangle$ is the mean squared average of the background electron velocity fluctuations associated with the electric fields in the turbulence, and τ is the correlation time of the fluctuations. Since μ is typically $0.01c^2/\omega_{pe}$ in the present simulation, the decay time of $\langle B_z^2\rangle$ is evaluated to be $1/(2k^2\mu) = 50/\omega_{pe} \approx 8T_0$.

As in the previous simulation results [21], after the nonlinear damping, the energy $\langle B_z^2\rangle$ reaches a quasisteady state with a quite slow growth due to the remaining electron anisotropy [22] in the case without $\mathbf{B}_0$ or with strong $\mathbf{B}_0$. However, in the weak external magnetic field case, the energy $\langle B_z^2\rangle$ starts to grow anomalously on a time scale much longer than $1/\omega_{pe}$ after the nonlinear decay. In a longer-time ($120T_0$) simulation, it is found that this growth would stop at about $66T_0$ when the beam electrons are fully thermalized. The final energy $\langle B_z^2\rangle$ in the $\mathbf{B}_0 = 0.15$ case is nearly one order of magnitude higher than the other cases as shown in Fig. 1(a). Further, compare the momentum spread of the beam and background electrons in the unmagnetized and weakly magnetized cases. It is found that the beam electrons are significantly decelerated and the background electrons strongly heated up in the weakly magnetized case, and about 5.4% more total beam energy is lost in the weakly magnetized than that in the unmagnetized case.

A. Generation and propagation of MDs

To understand the mechanism of the unusual nonlinear growth of $\langle B_z^2\rangle$ as well as the anomalous energy dissipation of the beam electrons for the weakly magnetized case, we first look into the dynamics of the magnetic field fluctuations. Initially, in the linear stage, the distributions of the magnetic fluctuations are similar for $\mathbf{B}_0 = 0$ and $\mathbf{B}_0 = 0.15$, which reveals that the fluctuations associating with the WI and TSI propagate obliquely. Then the inverse cascade begins with current filamentation and the scales of the magnetic fluctuations become larger. Figures 2(a), 2(c), and 2(e) show snapshots of the B_z field fluctuations at $t = 14T_0$ for the three

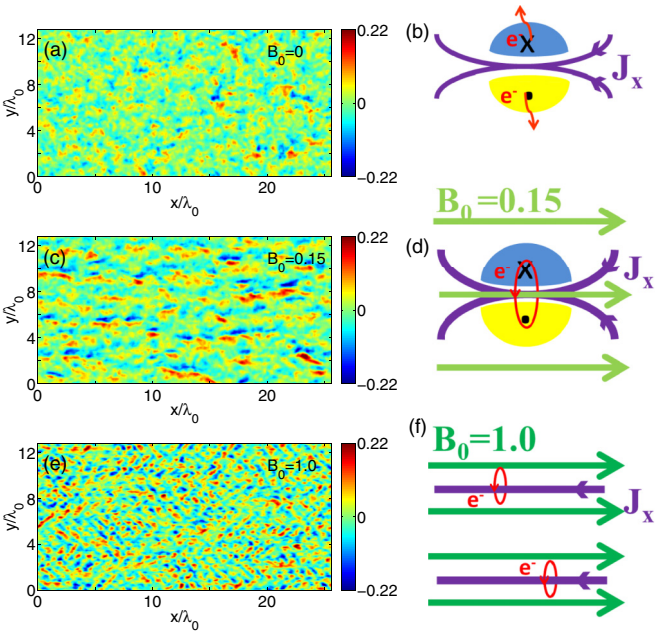

FIG. 2. (Color online) Snapshots of the magnetic field B_z at $t = 14T_0$. (a), (c), and (e) are for $\mathbf{B}_0 = 0$, $\mathbf{B}_0 = 0.15$, and $\mathbf{B}_0 = 1.0$, respectively. (b), (d), and (f) are the sketches for the three cases, respectively. The blue and yellow regions in (b) and (d) denote the magnetic dipoles, and the red curves (circles) denote the irregular thermal motion (cyclotron motion) of electrons.

cases. We can observe small MD-like structures appearing in both the unmagnetized [Fig. 2(a)] and weakly magnetized [Fig. 2(c)] cases. These small MD seeds come from the possible merging and crossing of current filaments [see Figs. 2(b) and 2(d)], since the magnetic fluctuations correspond to the current fluctuations. In the unmagnetized case, such small structures just appear instantaneously at the time of crossing, and disappear quickly due to magnetic dissipation by electron thermal motions [denoted by the red curves in Fig. 2(b)]. Conversely, in the finite external magnetic field case, the MD seeds are made more parallel by the guiding of $\mathbf{B}_0$, and because of the cyclotron motion of electrons [denoted by the red circles in Fig. 2(d)], these small structures can survive for a long enough time to grow up and finally self-organize the coherent MDs shown in Fig. 3(a). The growth of MD seeds and the formation of MDs are coincident with the slow nonlinear increase of energy $\langle B_z^2 \rangle$. On the other hand, in the strong external magnetic field case [Figs. 2(e) and 2(f)], the electron cyclotron radius is so small that the neighboring filaments are fully isolated and do not interact with each other. Consequently the dipolelike structures do not appear. Thus, the external magnetic field is critical for the formation of MDs. Under our present system parameters, the self-organized MDs can be observed only when the external magnetic field amplitude is in the range $0.05 \leqslant \mathbf{B}_0 \leqslant 0.3$.

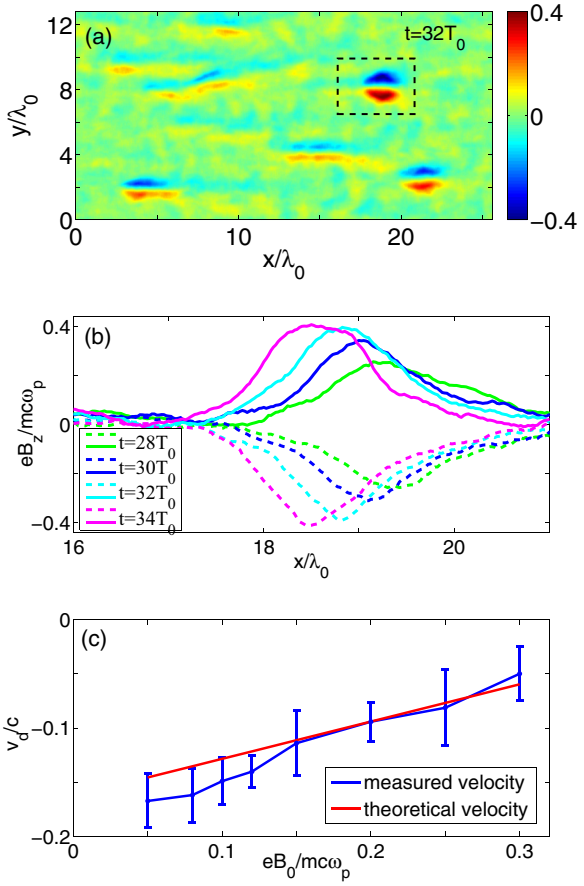

FIG. 3. (Color online) (a) Snapshot of the B_z field distribution at $t = 32T_0$ for the $\mathbf{B}_0 = 0.15$ case. (b) The profile of B_z versus $\mathbf{x}$ for fixed $y = 7.6\lambda_0$ (solid line) and $y = 8.1\lambda_0$ (dashed line) at different times $t = 28T_0, 30T_0, 32T_0$, and $34T_0$. (c) Measured average drift velocities and theoretical velocities of the dipoles for different amplitudes of the external magnetic field.

In the $\mathbf{B}_0 = 0.15$ case, we observe that the self-organized dipoles drift in the negative x direction at a quasisteady velocity, and the amplitude of the dipole gradually increases during the drift. Such dynamics is clearly illustrated in Fig. 3(b) in terms of the magnetic profiles at four different times. It is plotted along the horizontal cut at $y = 7.6\lambda_0$ and $y = 8.1\lambda_0$ of the dipole marked by the broken line in Fig. 3(a). These dipoles propagate stably for at least $30T_0$ in this case. The observed drift velocity $\mathbf{v}_d$ depends on the external magnetic field as is exhibited in Fig. 3(c) (blue line).

In order to elucidate the effect of the external magnetic field on the motion of MDs, we resort to the theory of electron magnetohydrodynamics (EMHD), which is applicable to describing the magnetized electron fluid when the time scale is fast enough to allow the ion motions to be ignored. Since the electromagnetic perturbations vary in the two-dimensional simulation plane, the governing equations of 2D EMHD can be written in terms of two scalar variables b and ψ as [23]

$$\frac{\partial}{\partial t}(\psi - \nabla^2\psi) + \hat{z} \times \nabla b \cdot (\psi - \nabla^2\psi) = S1, \tag{1}$$

$$\frac{\partial}{\partial t}(b - \nabla^2 b) - \hat{z} \times \nabla b \cdot \nabla(\nabla^2 b) + \hat{z} \times \nabla\psi \cdot \nabla(\nabla^2\psi) = S2. \tag{2}$$

Here the source terms ($S1$ and $S2$) denote the kinetic effects of the beam electrons, which are neglected in the following discussions, since the density of beam electrons is much lower than that of the background electrons. Considering the external magnetic field $B_0\hat{x}$, we can assume $\psi = -B_0 y + \varphi$, and thus the total magnetic field is $\mathbf{B} = B_0\hat{x} + \hat{z} \times \nabla\varphi + b\hat{z}$. Based on the point vortex model [24], we choose $\nabla^2\varphi = -k^2\varphi$ and $\nabla^2 b = -k^2 b$ in the neighborhood of the vortex center, where k is the curvature of the B_z field profile at the vortex center $[(x_0, y_0) = (18.8\lambda_0, 7.6\lambda_0)$ or $(18.8\lambda_0, 8.1\lambda_0)$ for the marked dipole in Fig. 3(a)]. Since the MDs drift in the negative x direction at a quasisteady translational velocity $\mathbf{v}_t$, it is reasonable to assume that b and φ are functions of $(x - v_t t)$ and y only. We integrate these equations around the center of one vortex and, after some straightforward algebra, we can obtain the relationship between the translational velocity of the MDs and the external magnetic field as

$$v_t = -\left(\frac{\partial b}{\partial y}\right)_{(x_0, y_0)} + \frac{k}{1 + k^2} B_0. \tag{3}$$

Here the subscript (x_0, y_0) represents taking the magnetic gradient at the center of one vortex of the dipole, which is approximately proportional to the dipole amplitude. The average drift velocities of the MDs measured in simulations with different external magnetic field amplitudes (blue line) are compared with the velocity given by Eq. (3) (red line) for $k = 0.4$ in Fig. 3(c), where the magnetic field gradient, namely, the first term of Eq. (3), is assumed to be small and is neglected. Note that the actual drift velocity observed in the laboratory frame should be $\mathbf{v}_d = \mathbf{v}_b + \mathbf{v}_t$ where the background flow velocity is $\mathbf{v}_b = -0.163c$. It is found that the offset linear dependence of the measured drift velocity on

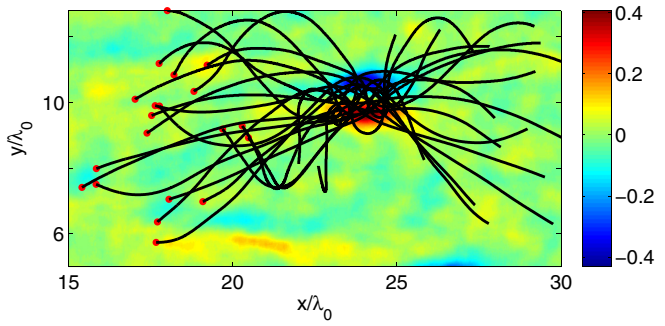

FIG. 4. (Color online) The trajectories of sampled beam electrons based on the B_z structure. The red points are starting points.

the external magnetic field amplitude agrees approximately with the EMHD analysis.

B. Amplification of the MDs and the anomalous energy dissipation

Next, we investigate the dynamics of electrons around the MDs to look for the mechanism of the anomalous energy dissipation of the beam electrons. Figure 4 shows part of the trajectories of some sampled beam electrons passing through the typical MD marked in Fig. 3(a). It is clear that due to the large magnetic amplitude of the dipole, the beam electrons moving forward are deflected and focused by the Lorentz force $-ev_xB_z$. Similarly, the background electrons moving backward are scattered out of the MD. Thus, the beam electron density is high in the MD [see Fig. 5(a)] while the background electron density is depleted [see Fig. 5(b)]. Comparing the relative density variations of the beam and background electrons, we find that the overall electron density is reduced in the MD as a result of the above scattering process. Thus a positive electrostatic potential well is excited accordingly, and the detailed structures of the electric field E_x and E_y are shown in Figs. 5(c) and 5(d). The peripheral electric fields around the MD are the electrostatic components resulting from the positive potential well, the structures of which are similar to the analytic magnetic bisoliton solutions provided by Bychenkov [25] and the MDs observed in the laser wake field in the simulations by Nakamura [12]. It is worth noting that there is a positive E_x component in the center of the MD as marked by the dashed elliptical

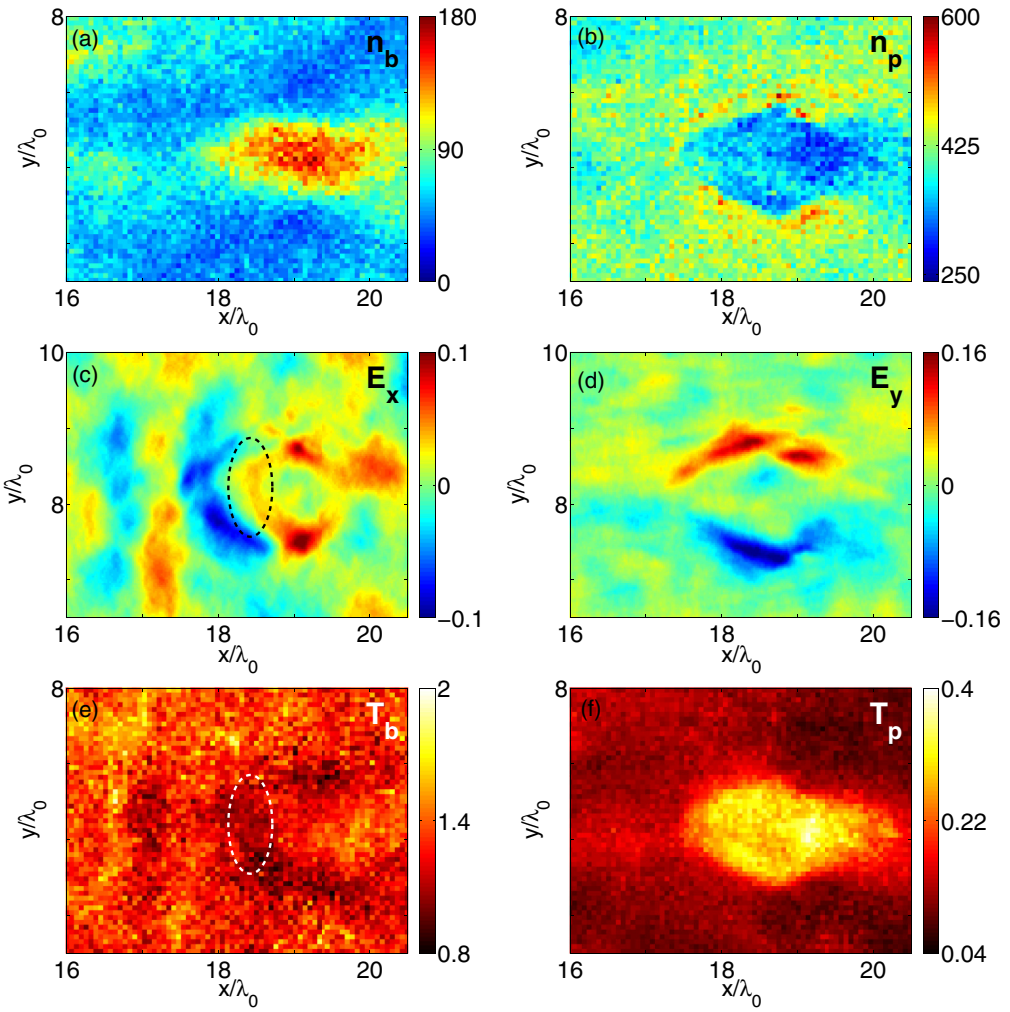

FIG. 5. (Color online) (a) and (b) represent respectively the density distribution of the beam and background electrons at $32T_0$ in the marked dipole region respectively. (c) and (d) represent the detail electric field E_x and E_y in the same region respectively. (e) and (f) represent the corresponding average energy (unit: MeV) per electron for the beam and background electrons respectively.

line in Fig. 5(c). This field is the inductive electromagnetic component $\frac{\partial B_z}{\partial t} = -\frac{\partial E_{y,\mathrm{ind}}}{\partial x} + \frac{\partial E_{x,\mathrm{ind}}}{\partial y}$ when the MD grows, and it contributes to decelerating the beam electrons. Look at the average energy (i.e., the effective temperature) distribution of the beam and background electrons in the same MD region shown in Figs. 5(e) and 5(f). The average energy is lower for the beam electrons around the MD than for those outside the MD, and the deceleration region corresponds to the electromagnetic E_x component. In addition, the average energy of the background electrons is very high in the MD as shown in Fig. 5(f), which is because some low-energy background electrons are trapped by the positive potential well, and gradually accelerated during the oscillatory motions inside the well by the inductive electric fields associated with the amplification of B_z.

From the above observations and analysis, the generation mechanism and dynamics of the MDs in a weak external magnetic field are summarized as follows. First, tiny current filaments are developed by the WI together with the TSI, and the microfilaments are dissipated by an inverse cascade and the anomalous viscosity after the saturation of the instabilities. Then, mesoscale current filaments are dominant and maintained by the weak external magnetic field. In the second stage, the crossing and merging of these current filaments start to amplify the magnetic field B_z at the crossing points as shown in Fig. 2(b). The strong B_z fields around the filament merging points focus the beam electrons, which further strengthen the local current amplitude and the electromagnetic fields. Thus the MDs are gradually self-organized and grow. During the amplification of the B_z field, the electromagnetic E_x field is generated inductively and decelerates the beam electrons. The energy lost by the beam is transferred to the electromagnetic field energy and the kinetic energy of the trapped background electrons. The kinetic energy of these trapped background electrons will become thermal energy when the MDs break up. These processes give a whole account of the anomalous beam energy dissipation in a weak external magnetic field.

III. PARTICLE-IN-CELL SIMULATION FOR LASER-PLASMA INTERACTION

To validate our conclusions in realistic laser plasmas, we simulate the interaction of an ultraintense laser pulse with a preionized electron–carbon-ion plasma with the ASCENT code. Linearly polarized laser light with an intensity of 1×10^{19} W cm^{-2} is incident from the left side; its amplitude rises in $1T_L$ ($T_L = 2\pi/\omega_L$ is the laser period, and ω_L is the laser center frequency) and then remains constant. The slab target with a density of $9n_c$ ($n_c = m_e\omega_L^2/4\pi e^2$) is located from $4\lambda_L$ ($\lambda_L = 2\pi c/\omega_L = 1.06$ μm is the laser wavelength) to $40\lambda_L$. Absorbing boundary conditions are adopted for both the left and right sides. The transverse scale of the target is $15\lambda_L$ and a periodic boundary is still used in the y direction. We compare the case without and with an external magnetic field of $\mathbf{B}_0 = 40$ MG (so that $\omega_c/\omega_{pe} = 0.13$).The ions are kept immobile during the total simulation time of $100T_L$.

Figure 6(a) and 6(b) show snapshots of the self-generated B_z field at the time $t = 80$ fs for the two cases; the corresponding distributions of the effective temperature of the electrons at the same time are shown in Figs. 6(c) and 6(d). From these results, we can clearly observe that MDs are formed, fast electrons remain near the laser-plasma interaction surface,

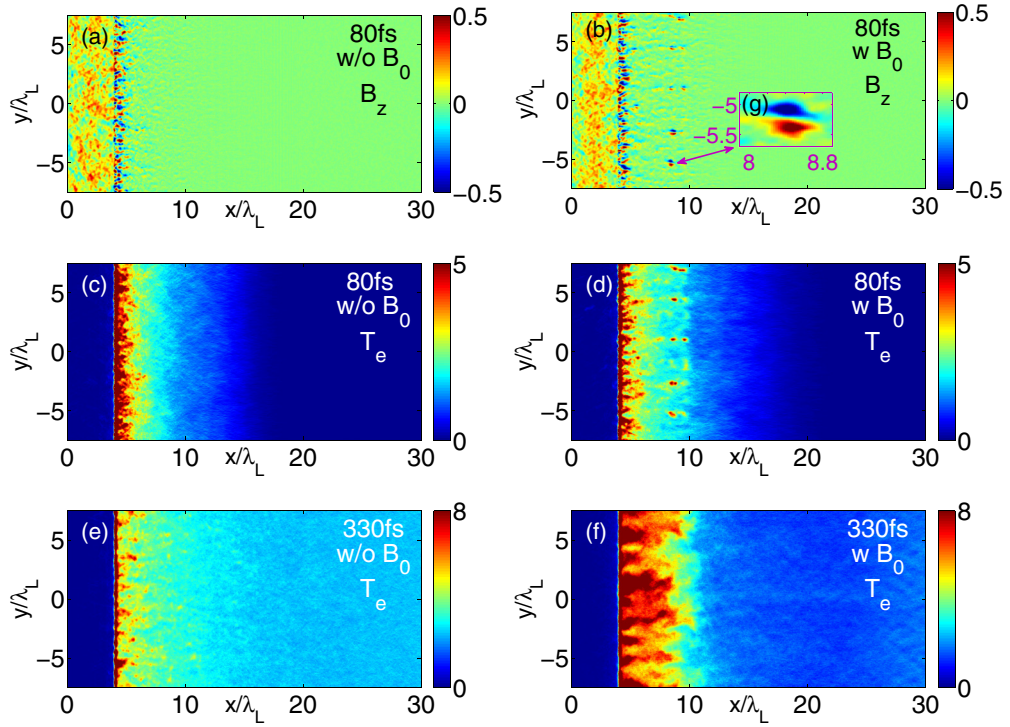

FIG. 6. (Color online) (a) and (b) are snapshots of the magnetic field B_z (units of 100 MG) for the cases without and with $\mathbf{B}_0$ at $t = 80$ fs. The inset figure (g) in (b) is the amplification of the MD directed by the arrow. (c) and (d) are the electron energy density (units of $n_c m_e c^2$) distributions at $t = 80$ fs. (e) and (f) are the electron energy density distributions at $t = 330$ fs.

and the electron energy density becomes extremely high in the MD area for the weakly magnetized case. The typical scale of these MDs is about the electron skin depth, as is shown in Fig. 6(g), a plot of the amplified detailed structure of one MD in Fig. 6(b). These MDs move back to the laser-plasma interaction region quickly after formation, the same as is observed in the former pure counterstreaming system. At the later time, more high-energy electrons are trapped near the interaction surface in the weakly magnetized case compared with the unmagnetized case, as shown in Figs. 6(e) and 6(f). All these results therefore indicate that MDs in the weakly magnetized system and the resultant enhanced electron energy dissipation due to the strong electromagnetic fluctuations associated with the MDs are ubiquitous.

IV. SUMMARY

In summary, we have studied the elementary physics of self-organized MDs and the corresponding continued increase of the self-generated magnetic field in the nonlinear evolution stage of the instability in a weakly magnetized beam-plasma system. Starting with the EMHD equations, it is found that the dipoles drift with a velocity depending on the magnetic amplitude of the dipole and the amplitude of the external magnetic field. Our PIC simulation results are consistent with the EMHD analysis. It is also demonstrated that the MDs serve as a medium for energy transfer between the beam and background electrons. According to this anomalous energy dissipation mechanism, as also verified in the laser-plasma interaction simulations, we suggest that the Weibel-instability-mediated collisionless shock could be much stronger in weakly magnetized plasmas and additional phenomena could be explored in the collisionless shock acceleration of ions, relevant studies on which are in progress and will be presented elsewhere.

ACKNOWLEDGMENTS

We would like to kindly acknowledge useful discussions with M. Hata, H. Sakagami, T. Nakamura, and A.Sunahara, and give many thanks for the comments and suggestions by the referees for improving our work. This work is supported by the China Scholarship Council (CSC) and the National Natural Science Foundation of China (Grant No. 11275028). Simulations are supported by the Cyber Media Center and Institute of Laser Engineering of Osaka University.

[1] D. Bohm and E. P. Gross, Phys. Rev. **75**, 1851 (1949).

[2] E. S. Weibel, Phys. Rev. Lett. **2**, 83 (1959); B. Fried, Phys. Fluids **2**, 337 (1959); A. Bret, M. C. Firpo, and C. Deutsch, Phys. Rev. Lett. **94**, 115002 (2005); A. Bret, L. Gremillet, D. Bénisti, and E. Lefebvre, *ibid.* **100**, 205008 (2008).

[3] M. Honda, J. Meyer-ter-Vehn, and A. Pukhov, Phys. Rev. Lett. **85**, 2128 (2000); Y. Sentoku, K. Mima, P. Kaw, and K. Nishikawa, *ibid.* **90**, 155001 (2003).

[4] J. C. Adam, A. Héron, and G. Laval, Phys. Rev. Lett. **97**, 205006 (2006); A. Debayle, J. J. Honrubia, E. d'Humières, and V. T. Tikhonchuk, Phys. Rev. E **82**, 036405 (2010).

[5] L. O. Silva, R. A. Fonseca, J. W. Tonge, J. M. Dawson, W. B. Mori, and M. V. Medvedev, Astrophys. J. **596**, L121 (2003); M. Medvedev, M. Fiore, R. Fonseca, L. Silva, and W. Mori, *ibid.* **618**, L75 (2005); K.-I. Nishikawa, P. E. Hardee, C. B. Hededal, and G. J. Fishman, *ibid.* **642**, 1267 (2006).

[6] L. Sironi and A. Spitkovsky, Astrophys. J. **698**, 1523 (2009).

[7] H. Daido, F. Miki, K. Mima, M. Fujita, K. Sawai, H. Fujita, Y. Kitagawa, S. Nakai, and C. Yamanaka, Phys. Rev. Lett. **56**, 846 (1986); H. Daido, K. Mima, F. Miki, M. Fujita, Y. Kitagawa, S. Nakai, and C. Yamanaka, Jpn. J. Appl. Phys. **26**, 1290 (1987); P. Y. Chang, G. Fiksel, M. Hohenberger, J. P. Knauer, R. Betti, F. J. Marshall, D. D. Meyerhofer, F. H. Seguin, and R. D. Petrasso, Phys. Rev. Lett. **107**, 035006 (2011); H. Daido, Y. Kato, K. Murai, S. Ninomiya, R. Kodama, G. Yuan, Y. Oshikane, M. Takagi, H. Takabe, and F. Koike, *ibid.* **75**, 1074 (1995); S. Fujioka, Z. Zhang, K. Ishihara, K. Shigemori, Y. Hironaka, T. Johzaki, A. Sunahara, N. Yamamoto, H. Nakashima, T. Watanabe, H. Shiraga, H. Nishimura, and H. Azechi, Sci. Rep. **3**, 1170 (2013); L. Giuffrida, in Proceedings of the 41st EPS Conference on Plasma Physics (to be published).

[8] D. J. Strozzi, M. Tabak, D. J. Larson, L. Divol, A. J. Kemp, C. Bellei, M. M. Marinak, and M. H. Key, Phys. Plasmas **19**, 072711 (2012); Hong-bo Cai, Shao-ping Zhu, and X. T. He, *ibid.* **20**, 072701 (2013).

[9] K. Mima, in Proceedings of the 12th International Workshop on Fast Ignition of Fusion Targets (to be published).

[10] F. Fiuza, R. A. Fonseca, J. Tonge, W. B. Mori, and L. O. Silva, Phys. Rev. Lett. **108**, 235004 (2012).

[11] S. V. Bulanov, M. Lontano, T. Z. Esirkepov, F. Pegoraro, and A. M. Pukhov, Phys. Rev. Lett. **76**, 3562 (1996); S. V. Bulanov, T. Esirkepov, M. Lontano, and F. Pegoraro, Plasma Phys. Rep. **23**, 660 (1997).

[12] T. Nakamura and K. Mima, Phys. Rev. Lett. **100**, 205006 (2008); T. Nakamura, S. V. Bulanov, T. Z. Esirkepov, and M. Kando, *ibid.* **105**, 135002 (2010).

[13] F. Califano, F. Pegoraro, and S. V. Bulanov, Phys. Rev. Lett. **84**, 3602 (2000).

[14] A. Das and P. H. Diamond, Phys. Plasmas **7**, 170 (2000); P. H. Diamond, A. Hasegawa, and K. Mima, Plasma Phys. Controlled Fusion **53**, 124001 (2011).

[15] T. Taguchi, in Proceedings of the 8th International Conference on Inertial Fusion Science and Applications (to be published).

[16] F. Fiuza, A. Stockem, E. Boella, R. A. Fonseca, L. O. Silva, D. Haberberger, S. Tochitsky, C. Gong, W. B. Mori, and C. Joshi, Phys. Rev. Lett. **109**, 215001 (2012).

[17] Hong-bo Cai, K. Mima, Wei-min Zhou, T. Jozaki, H. Nagatomo, A. Sunahara, and Rodney J. Mason, Phys. Rev. Lett. **102**, 245001 (2009).

[18] Y. Sentoku and A. J. Kemp, J. Comput. Phys. **227**, 6846 (2008).

[19] K. F. Lee, Phys. Rev. Lett. **21**, 1439 (1968); K. Molvig, *ibid.* **35**, 1504 (1975); A. Bret, M. E. Dieckmann, and C. Deutsch, Phys. Plasmas **13**, 082109 (2006).

[20] H. Xie, Comput. Phys. Commun. **185**, 670 (2014).
[21] R. A. Fonseca, L. O. Silva, J. W. Tonge, W. B. Mori, and J. M. Dawson, Phys. Plasmas **10**, 1979 (2003); D. V. Romanov, V. Yu. Bychenkov, W. Rozmus, C. E. Capjack, and R. Fedosejevs, Phys. Rev. Lett. **93**, 215004 (2004).
[22] L. Gremillet, D. Benisti, E. Lefebvre, and A. Bret, Phys. Plasmas **14**, 040704 (2007).
[23] D. Biskamp, E. Schwarz, and J. F. Drake, Phys. Rev. Lett. **76**, 1264 (1996); S. Dastgeer, A. Das, P. Kaw, and P. H. Diamond, Phys. Plasmas **7**, 571 (2000).
[24] A. Das, Plasma Phys. Controlled Fusion **41**, A531 (1999).
[25] V. Yu. Bychenkov, V. P. Silin, and V. T. Tikhonchuk, Theo. Math. Phys. **82**, 11 (1990).